Ionics (2015) 21:1835–1842
DOI 10.1007/s11581-015-1371-9

ORIGINAL PAPER

Enhanced high-temperature cycling stability of $LiNi_{1/3}Co_{1/3}Mn_{1/3}O_2$-coated $LiMn_2O_4$ as cathode material for lithium ion batteries

Jing Yan · Haohan Liu · Yuelei Wang · Xinxin Zhao · Yiming Mi · Baojia Xia

Received: 19 August 2014 / Revised: 23 December 2014 / Accepted: 13 January 2015 / Published online: 10 February 2015

Abstract To enhance the electrochemical performances of $LiMn_2O_4$ at elevated temperature, we proposed a sol–gel method to synthesize $LiNi_{1/3}Co_{1/3}Mn_{1/3}O_2$-modified $LiMn_2O_4$. The physical and electrochemical performances of pristine and $LiNi_{1/3}Co_{1/3}Mn_{1/3}O_4$-coated $LiMn_2O_4$ cathode materials were investigated by X-ray diffraction, scanning electron microscopy, transmission electron microscopy, X-ray photoelectron spectroscopy, and electrochemical measurements, respectively. The results indicated that about 5–6-nm-thick layer of $LiNi_{1/3}Co_{1/3}Mn_{1/3}O_2$ formed on the surface of the $LiMn_2O_4$ powders. The modified $LiMn_2O_4$ exhibited excellent storage performance at 45, 55, and 65 °C compared to the pristine one, which was attributed to the suppression of electrolyte decomposition and the reduction of Mn dissolution.

Keywords $LiMn_2O_4$ · Sol–gel method · Surface coating · Electrochemical performance

Introduction

With the advantages of being abundant, nontoxic, and inexpensive, spinel lithium manganese oxide ($LiMn_2O_4$) is a promising candidate for layered cathode materials such as $LiCoO_2$ [1, 2]. Especially, the good stability of $LiMn_2O_4$ may ensure its large-scale usage in batteries for electric vehicle or energy storage [3]. However, $LiMn_2O_4$ shows obvious capacity fade when cycling at high temperature (50–60 °C) [4–6]. It was reported that the capacity fading mechanism at high temperature was related to the Jahn–Teller distortion and dissolution of Mn^{2+} ions [7, 8]. Mn dissolution is induced by HF acid, which is generated by secondary chemical reactions from temperature-enhanced electrolyte decomposition.

In order to solve this problem, earlier studies have been focused on the chemical modification of $LiMn_2O_4$ by a partial substitution of Mn with some metal ions to obtain $LiM_xMn_{2-x}O_4$ (M=Co, Mg, Cr, Ni, Fe, Al, Ti, and Zn) [9–12]. These results indicated that the substitution of Mn with metal ions significantly improved the cycle performance of $LiMn_2O_4$. However, the partial substitutions decrease the capacity of $LiMn_2O_4$. Another effective way is surface coating on $LiMn_2O_4$ by an oxide with high thermal and structural stability. ZrO_2, SiO_2, Al_2O_3, and MgO [13–16] have been used to coat $LiMn_2O_4$ by some chemical processes. Nevertheless, the aforementioned oxides do not have de-intercalation and intercalation of Li ions, which will result in a decrease in initial capacity. Additionally, proper lithium ion conductivity is a fundamental parameter used to choose the coating materials. $LiNi_{1/3}Co_{1/3}Mn_{1/3}O_2$ has de-intercalation and intercalation of Li ions, which may suppress the dissolution of Mn. Therefore, it is expected that the modified $LiMn_2O_4$ will show an excellent cycle performance at elevated temperature. In this study, we proposed an approach to synthesize $LiNi_{1/3}Co_{1/3}Mn_{1/3}O_2$ on the surface of spinel $LiMn_2O_4$. The effects of the $LiNi_{1/3}Co_{1/3}Mn_{1/3}O_2$ layer on the morphology and electrochemical performances of $LiMn_2O_4$ cathode materials were examined in detail.

J. Yan · Y. Wang · X. Zhao · Y. Mi (✉)
College of Chemistry and Chemical Engineering, Shanghai University of Engineering Science, Shanghai 201620, China
e-mail: theflyingdutchmen@163.com

H. Liu
Shanghai Nanotechnology Promotion Center, Shanghai 200237, China

H. Liu · B. Xia
Shanghai Institute of Microsystem and Information Technology, Chinese Academy of Sciences, Shanghai 20050, China

Experimental

$LiMn_2O_4$ powder was purchased from Hebei Strong-Power Li-ion Battery Technology Co., Ltd. (D98, China). To coat $LiMn_2O_4$ with $LiNi_{1/3}Co_{1/3}Mn_{1/3}O_2$, $LiCH_3COO \cdot 2H_2O$ (1.057 g), $Mn(CH_3COO)_2 \cdot 4H_2O$ (0.85 g), $Ni(CH_3COO)_2 \cdot 4H_2O$ (0.86 g), and $Co(CH_3COO)_2 \cdot 4H_2O$(0.86 g) with a stoichiometric ratio of 3:1:1:1 were dissolved in distilled water to form a clear solution. An aqueous solution of ethylene glycol and citric acid as a chelating agent was added to the mixtures. pH value at 7.0–7.5 was achieved using ammonium hydroxide. Then the $LiMn_2O_4$ powders (50 g) were slowly added to the sol and vigorously stirred at 85 °C for 8 h. The sol turned into viscous transparent gel when the water evaporated. After drying and sieving, the powder was sintered in air at 400 °C for 5 h and 750 °C for 3 h to obtain $LiNi_{1/3}Co_{1/3}Mn_{1/3}O_2$-coated $LiMn_2O_4$. For a comparison, pristine $LiMn_2O_4$ was also heat-treated in the same condition.

Structure and morphology characterization

X-ray diffraction (XRD) patterns were recorded on a DX-2700 diffractometer (Siemens D-5000, Mac Science MXP 18) equipped with Cu Kα radiation of λ=0.154145 nm. The diffraction patterns were recorded between scattering angles of 15° and 80° at a step of 4°/min. The morphology was studied using a scanning electron microscope (S4700, Hitachi) and transmission electron microscope (JEOL-1200EX). X-ray photoelectron spectroscopy (Kratos AXIS Ultra DLD) was employed to probe the surface for Mn valence states. After cycling, the batteries were disassembled in a glove box and the electrodes and membrane were washed with EC/DMC for several times. The cathode was used to examine the changes in structure by XRD, and the obtained solution was diluted to a suitable concentration to detect the content of Mn element. Inductively coupled plasma atomic emission spectrometry analysis was conducted on an IRIS Intrepid Π XSP inductively coupled plasma emission spectrometer (THERMO).

Electrochemical and thermal characteristics

To obtain working electrodes, 85 wt% active materials, 9 wt% acetylene black, and 6 wt% polyvinylidene fluoride were homogeneously mixed in *N*-methyl-pyrroline. Then the resulting slurry was spread on an aluminum foil and thoroughly dried. The electrodes were punched in the form of 14-mm-diameter disks, and the typical active material mass loading was about 6 mg/cm^2. The electrolyte was 1 M $LiPF_6$ dissolved in a mixture of ethylene carbonate and dimethylene carbonate with the volume ratio of 1:1. The anode of the battery is Li electrode. The assembly process was conducted in an argon-filled glove box with the content of H_2O and O_2 less than 1 ppm.

Before electrochemical tests, the batteries were aged for 24 h to ensure good soakage. The cells were charged and discharged on a battery tester (CT-3008 W, NEWARE) between 3.3 and 4.35 V at the rate of 2C at elevated temperatures in a dry oven (A201113, Shanghai). Cyclic voltammetry (CV) and electrochemical impedance spectroscopy (EIS) investigations were performed on an electrochemical workstation (PGSTAT302N, Autolab) at 25±2 °C. The CV curves were recorded between 3.3 and 4.35 V at a scan rate of 0.1 mV s^{-1}. The EIS measurements were performed over a frequency range from 10 kHz to 0.1 Hz.

Results and discussion

Figure 1 shows the XRD patterns of pristine and $LiNi_{1/3}Co_{1/3}Mn_{1/3}O_2$-coated $LiMn_2O_4$. The peaks of both samples could be indexed to a cubic spinel structure with the space group Fd3m. There is no substantial difference between XRD patterns for pristine and modified $LiMn_2O_4$. The crystal lattice parameters, which were calculated by using the software Jade, are 8.245 and 8.246 Å for the pristine and $LiNi_{1/3}Co_{1/3}Mn_{1/3}O_2$-coated $LiMn_2O_4$, respectively, indicating that the bulk structure of $LiMn_2O_4$ was unchanged after surface modification. The characteristic peaks corresponding to $LiNi_{1/3}Co_{1/3}Mn_{1/3}O_2$ are not observed because of low content (about 2.0 wt%).

Scanning electron microscopy reveals that the pristine and modified samples present a uniform particle distribution, ranging from 2 to 7 μm. The pristine spinel crystals are smooth with well-defined facets, as observed in Fig. 2a. It can be seen that the morphology and particle diameter of the $LiNi_{1/3}Co_{1/3}Mn_{1/3}O_2$-coated $LiMn_2O_4$ powders in Fig. 2b are similar to the pristine sample. No $LiNi_{1/3}Co_{1/3}Mn_{1/3}O_2$ agglomerations and obscured facets of spinel $LiMn_2O_4$ are observed.

The morphology of the modified sample is further analyzed by TEM measurement. As shown in Fig. 2c, about 5–6-nm-thick layer of $LiNi_{1/3}Co_{1/3}Mn_{1/3}O_2$ is uniformly formed on the surface of the $LiMn_2O_4$. The coating layer is clearly distinguishable from the crystalline $LiMn_2O_4$. To further identify the homogeneity of the coating layer, the element distribution is determined by energy-dispersive X-ray spectroscopy (EDS) mapping, which is displayed in Fig. 3. The dense accumulation of Mn element is attributed to the host material of $LiMn_2O_4$, and there is no significant agglomeration of Ni and Co. These results indicate that $LiNi_{1/3}Co_{1/3}Mn_{1/3}O_2$ is homogeneously dispersed on the surface of the $LiMn_2O_4$ particles.

The oxidation state of manganese ions at the surface was determined from X-ray photoelectron spectroscopy (XPS) data by the curve fitting of Mn 2p spectral peaks. The experimental peak shape for Mn $2p_{3/2}$ was modeled by employing

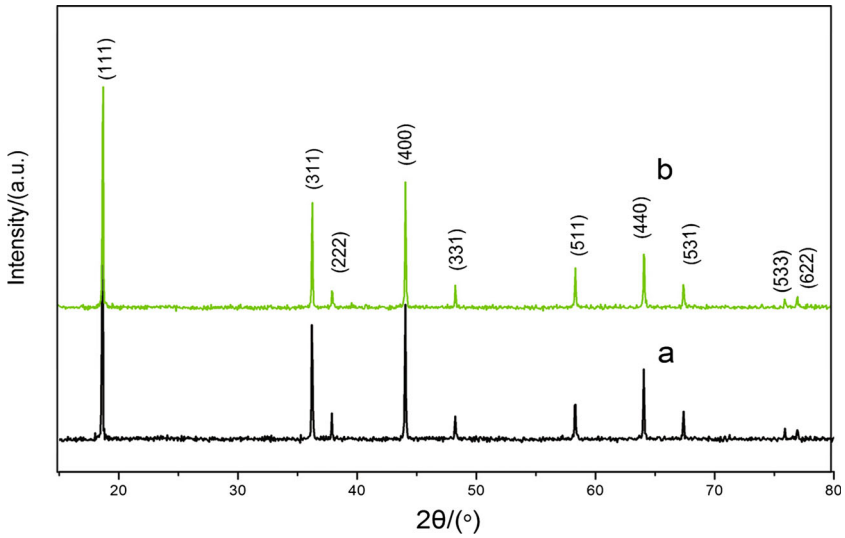

Fig. 1 X-ray diffraction patterns of (*a*) pristine and (*b*) $LiNi_{1/3}Co_{1/3}Mn_{1/3}O_2$-coated $LiMn_2O_4$

multiple-splitting patterns derived for Mn^{3+} and Mn^{4+} at binding energies of 641.6 and 642.8 eV from the standard compounds Mn_2O_3 and MnO_2. Figure 4 shows the fit of the models to the experimental spectra for pristine $LiMn_2O_4$ and $LiNi_{1/3}Co_{1/3}Mn_{1/3}O_2$-coated $LiMn_2O_4$, respectively. The surface of the pristine $LiMn_2O_4$ sample consists of almost equal amounts of Mn^{4+} and Mn^{3+} in Fig. 4a. By contrast, $LiNi_{1/3}Co_{1/3}Mn_{1/3}O_2$-coated $LiMn_2O_4$ exhibited a Mn^{4+}:Mn^{3+} ratio of 62.4:37.6 as shown in Fig. 4b. The difference in Mn^{4+}:Mn^{3+} ratio on the surface is due to the formation of $LiNi_{1/3}Co_{1/3}Mn_{1/3}O_2$ because it has a higher valence state of manganese ions. For a further comparison, the Ni 2p and Co 2p spectra of the samples are also studied, which are shown in Fig. 4c, d. For the pristine $LiMn_2O_4$ sample, there are no Ni 2p and Co 2p peaks. For the $LiNi_{1/3}Co_{1/3}Mn_{1/3}O_2$-coated $LiMn_2O_4$ sample, the Ni 2p region shows a Ni $2p_{3/2}$ main peak at 855.7 eV with a satellite peak at 862.1 eV, and the Co2p region shows a $Co2p_{3/2}$ main peak at 780.4 eV with a satellite peak at 796.8 eV. Combined with the difference in Mn 2p spectra, it is concluded that Ni^{2+} and Co^{3+} have deposited on the surface of $LiMn_2O_4$. This result is in good agreement with the observation in TEM and EDS element mapping.

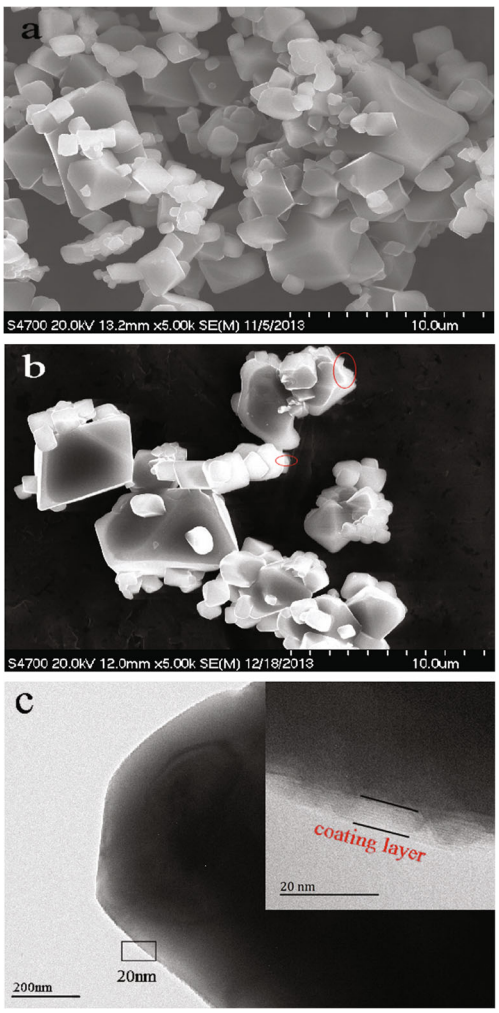

Fig. 2 SEM figures of **a** pristine and **b** $LiNi_{1/3}Co_{1/3}Mn_{1/3}O_4$-coated $LiMn_2O_4$ (the coating layer can be seen in the *red circles*) and **c** TEM figure of $LiNi_{1/3}Co_{1/3}Mn_{1/3}O_2$-coated $LiMn_2O_4$

The structure of pristine $LiMn_2O_4$ and $LiNi_{1/3}Co_{1/3}Mn_{1/3}O_2$-coated $LiMn_2O_4$ cathodes after cycling (55 °C) was examined. The results are given in Fig. 5. It can be seen that, compared with those of the pristine $LiMn_2O_4$ cathode, the diffraction peaks of the cycled $LiMn_2O_4$ cathode are obviously widened and the peak intensity declined. In addition, some extra peaks appear in the XRD pattern of the $LiMn_2O_4$ cathode after cycling, which should be assigned to $Li_2Mn_2O_4$. Usually, tetrahedral $Li_2Mn_2O_4$ can be generated at the final discharge stage of $LiMn_2O_4$ because of more Mn^{3+} and a more significant Jahn–Teller effect. On the other hand, for the $LiNi_{1/3}Co_{1/3}Mn_{1/3}O_2$-coated $LiMn_2O_4$ cathode, the diffraction peak width changed insignificantly before and after cycling. Compared with the fresh $LiNi_{1/3}Co_{1/3}Mn_{1/3}O_2$-coated $LiMn_2O_4$ cathode, in the XRD pattern of the cycled

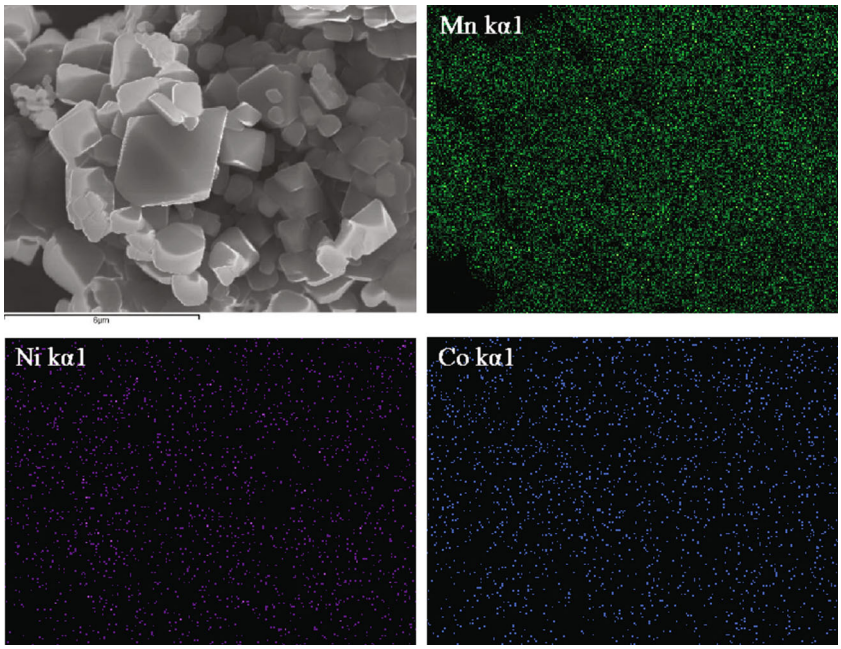

Fig. 3 EDS mappings of Ni, Co, and Mn elements of the modified $LiMn_2O_4$ sample

$LiNi_{1/3}Co_{1/3}Mn_{1/3}O_2$-coated $LiMn_2O_4$, the peak intensity declines slightly, which may be ascribed to the $LiNi_{1/3}Co_{1/3}Mn_{1/3}O_2$ on the surface of $LiMn_2O_4$.

Figure 6 shows the galvanostatic charge–discharge curves at different temperatures of (a) pristine and (b) $LiNi_{1/3}Co_{1/3}Mn_{1/3}O_2$-coated $LiMn_2O_4$ in a drying oven. The

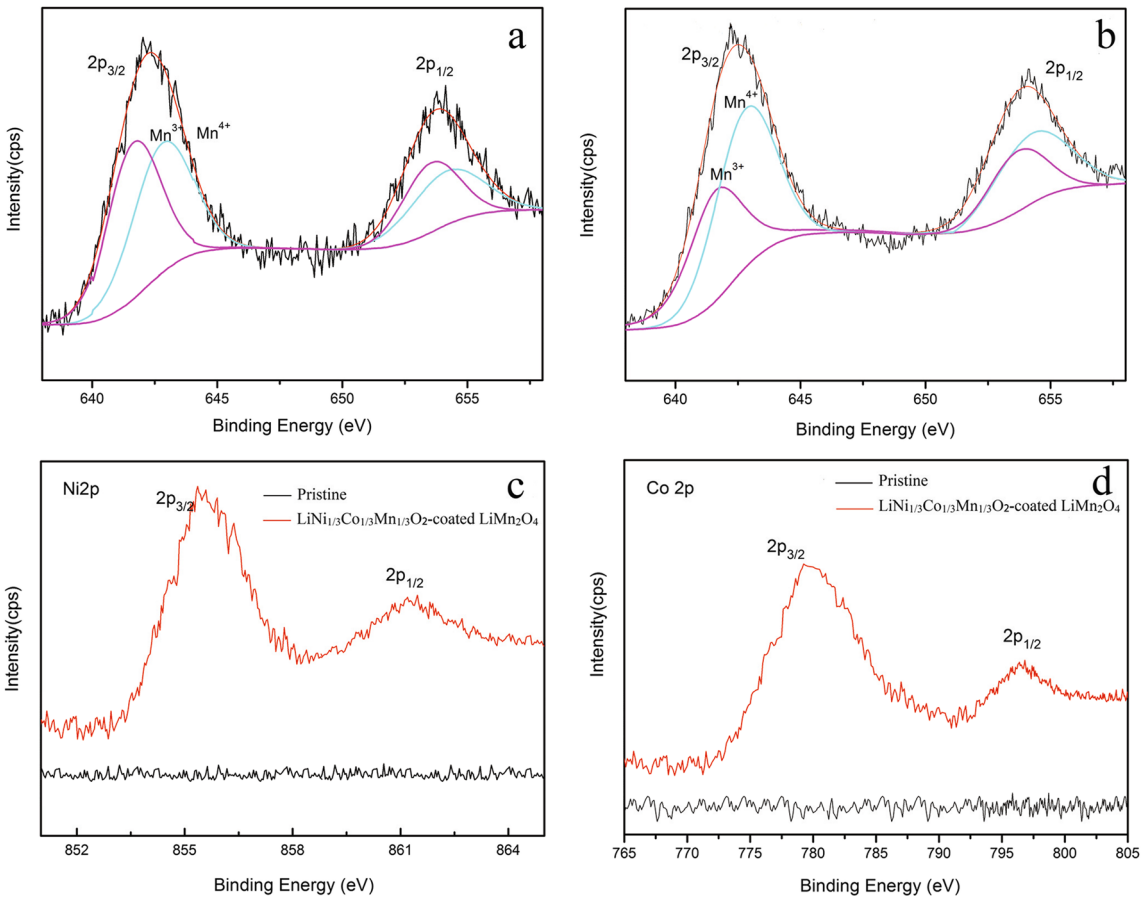

Fig. 4 **a** The Mn 2p XPS of pristine $LiMn_2O_4$ and the X-ray photoelectron spectra of $LiNi_{1/3}Co_{1/3}Mn_{1/3}O_2$-coated $LiMn_2O_4$ **b** Mn 2p, **c** Ni 2p, **d** Co 2p

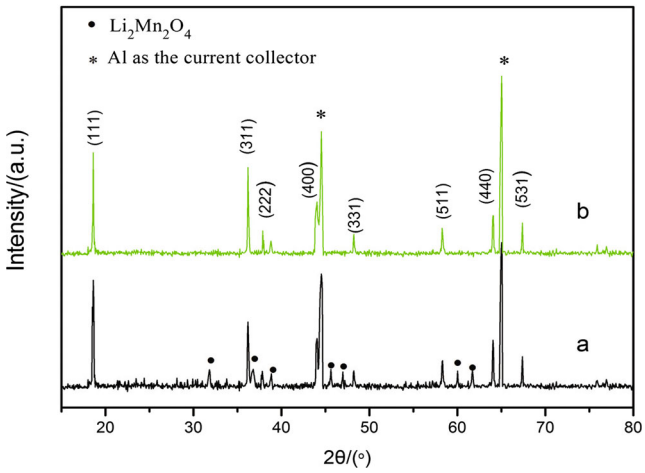

Fig. 5 XRD patterns of (*a*) pristine and (*b*) $LiNi_{1/3}Co_{1/3}Mn_{1/3}O_2$-coated $LiMn_2O_4$. The *asterisks* are Al as the current collector, and the *dots* are $Li_2Mn_2O_4$ which are produced in the charge and discharge processes

specific capacity increases with increased temperature, due to the higher lithium ion diffusion and lower resistance. Figure 6b shows two discharge plateaus, indicating that the

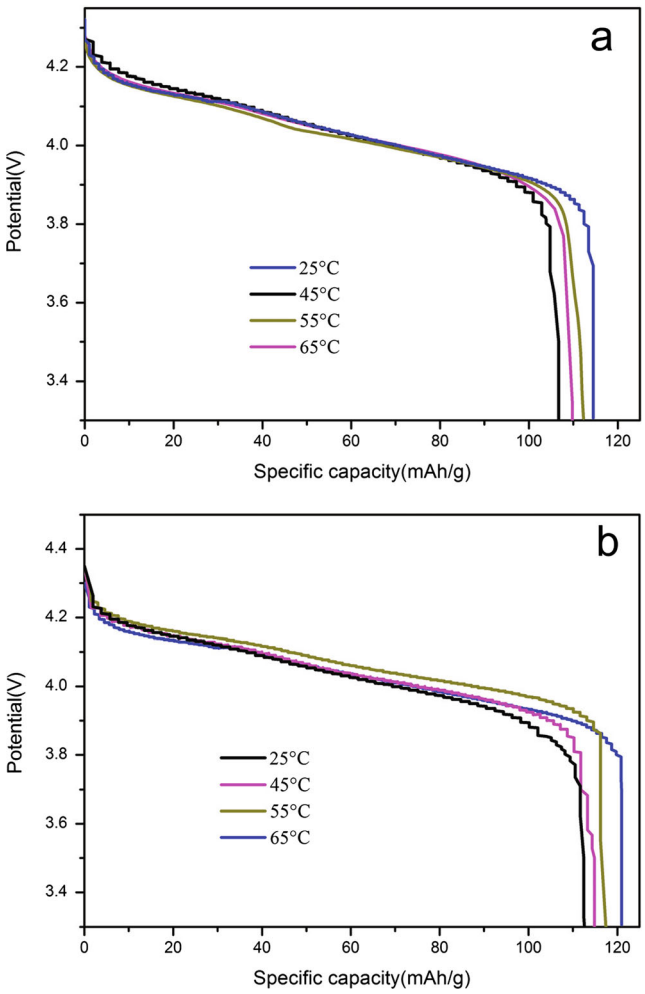

Fig. 6 The first charge–discharge curves at different temperatures of **a** pristine and **b** $LiNi_{1/3}Co_{1/3}Mn_{1/3}O_2$-coated $LiMn_2O_4$

$LiNi_{1/3}Co_{1/3}Mn_{1/3}O_2$ surface layer does not change the discharge mechanism of $LiMn_2O_4$ which orderly intercalates lithium ions in the tetrahedral (Fig. 6a) sites at 4.1 V and disorderly intercalates lithium ions at 3.9 V and which substantially maintains the intercalation feature of the $LiMn_2O_4$ substrate [17]; the two plateaus indicate the $LiNi_{1/3}Co_{1/3}Mn_{1/3}O_2$ surface layer rather than Ni-doped $LiMn_2O_4$ because $LiMn_2O_4$ with a Ni-doped spinel surface showed two ambiguously resolved discharging plateaus [18]. Meanwhile, $LiNi_{1/3}Co_{1/3}Mn_{1/3}O_2$-coated $LiMn_2O_4$ shows a higher discharge capacity compared to the pristine sample. The reason may be that $LiNi_{1/3}Co_{1/3}Mn_{1/3}O_2$ has higher capacity than $LiMn_2O_4$ with equivalent quality at this voltage range.

Figure 7 shows the cycling performance of electrodes with and without $LiNi_{1/3}Co_{1/3}Mn_{1/3}O_2$ coating at (a) 25±2 °C, (b) 45±2 °C, (c) 55±2 °C, and (d) 65±2 °C. After 100 cycles at room temperature, the capacity retention of the pristine sample (94.3 %) is similar to that of the modified sample (94.4 %), as shown in Fig. 7a. However, after 100 cycles at elevated temperature as shown in Fig. 7b–d, the capacity retention increases from 94.3 to 94.4 %, 88.7 to 93.5 %, 87.5 to 93.6 %, and 81.7 to 91 %, respectively. The three times repeat tests for the preparation of the modified sample are conducted, and the capacity retention is listed in Table 1. As shown in Fig. 7, the higher the temperature, the more retention rate improved. The reason might be that the side reactions at the interface of $LiMn_2O_4$ and electrolyte become more drastic at high temperature. Therefore, the protective effect of the coating layer becomes more significant. Compared with other coating materials such as Al_2O_3 [19], La_2O_3 [20], and $AlPO_4$ [21], surface modification by the sol–gel method can improve the high-temperature cycling stability of $LiMn_2O_4$ because the oxide layer can reduce the contact area of solid and electrolyte. However, the oxide itself is inactive with lithium ions and will result in a decrease in initial capacity. Compared to the oxide coating layer, $LiNi_{1/3}Co_{1/3}Mn_{1/3}O_2$ is more stable in the electrolyte than $LiMn_2O_4$ and has higher capacity. Thus, the electrode after coating has excellent cycle performance without reducing the initial capacity.

To further verify the effects of surface coating on manganese ion dissolution, the quality of the manganese element was directly determined by using ICP-AES. Li metal anode was washed with dilute hydrochloric acid after the 100th cycle at 55±2 °C. It can be seen in Table 2 that the dissolved quality of Mn^{2+} ions of the pristine and $LiNi_{1/3}Co_{1/3}Mn_{1/3}O_2$-coated $LiMn_2O_4$ electrodes was 22.54 and 10.17 μg/cm^2, respectively. It can be concluded that after coating by the $LiNi_{1/3}Co_{1/3}Mn_{1/3}O_2$ layer, the dissolution of the manganese ions was significantly reduced. Therefore, the $LiNi_{1/3}Co_{1/3}Mn_{1/3}O_2$-coated $LiMn_2O_4$ electrode had better cycle stability at elevated temperature. The reason might be that the valence state of Mn in $LiNi_{1/3}Co_{1/3}Mn_{1/3}O_2$ is +4,

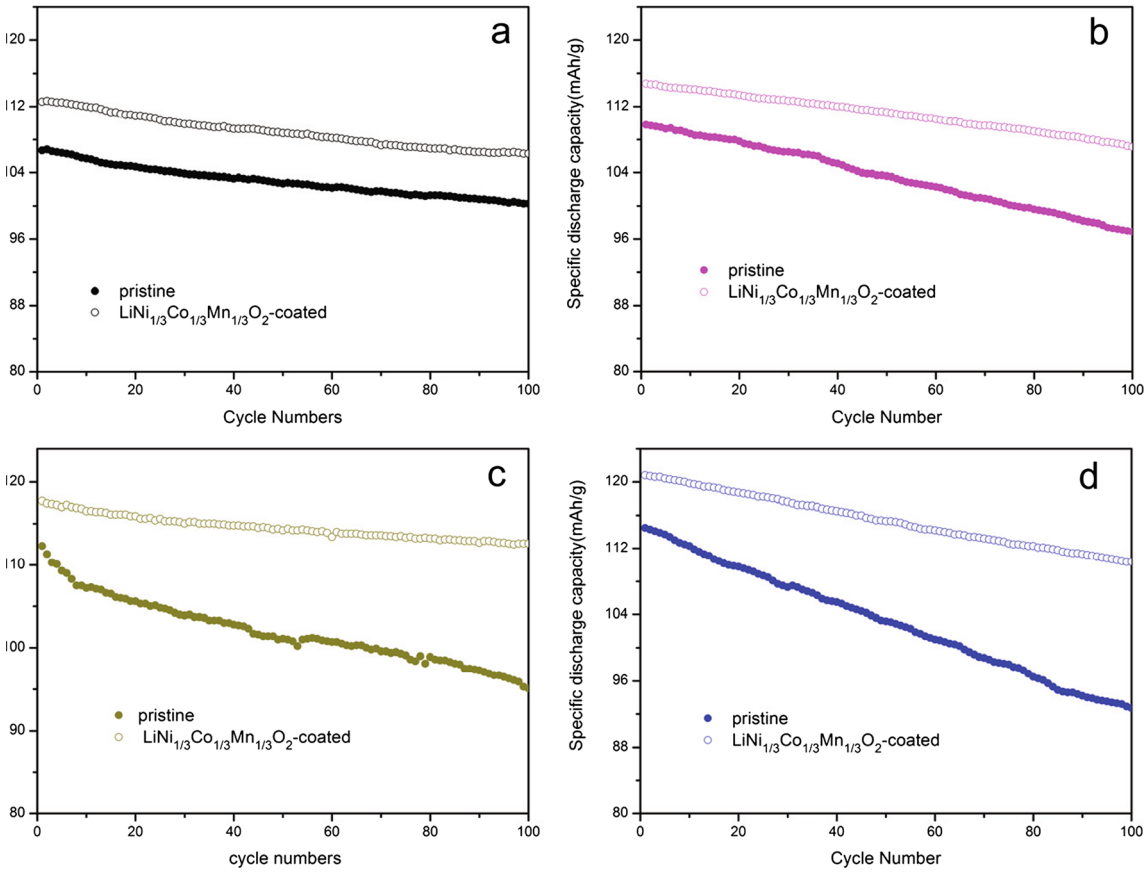

Fig. 7 Cycling behaviors at **a** 25±2 °C, **b** 45±2 °C, **c** 55±2 °C, and **d** 65±2 °C

which will suppress the Jahn–Teller effect on the surface of $LiMn_2O_4$. Another reason is that the coating material will reduce the contact area of $LiMn_2O_4$ and electrolyte, which may decrease the dissolution of Mn. The reactivity between $LiNi_{1/3}Co_{1/3}Mn_{1/3}O_2$ and electrolyte is not yet clear, which needs further research in the future.

Figure 8 shows the CV profiles of the pristine and $LiNi_{1/3}Co_{1/3}Mn_{1/3}O_2$-coated $LiMn_2O_4$ electrodes in the 10th and 100th cycles at the scan rate of 0.1 mV s^{-1}. The CV peaks of the $LiNi_{1/3}Co_{1/3}Mn_{1/3}O_2$-coated sample show two symmetrical couples of redox peaks at around 3.97 and 4.11 V, respectively (Fig. 8b), indicating that electrochemical insertion and extraction reactions of Li^+ ions are two step processes. It is in agreement with the two plateaus in Fig. 6 and demonstrates that $LiNi_{1/3}Co_{1/3}Mn_{1/3}O_2$ coating does not change the electrochemical reaction mechanism of $LiMn_2O_4$. After 10 cycles, two narrow and separate redox peaks appear around at 3.94 and 4.09 V, as shown in Fig. 8a. However, after the 100th cycle, due to the dissolution of Mn^{2+} ions into the electrolyte (Jahn-Teller distortion), both anodic and cathodic peaks become much broader and lower in peak current. In contrast, the oxidation and reduction peaks related to $LiNi_{1/3}Co_{1/3}Mn_{1/3}O_2$-coated $LiMn_2O_4$ are much steadier after 100 cycles (Fig. 8b), which indicated that modified $LiMn_2O_4$ has better reversibility and stability than the pristine $LiMn_2O_4$.

Electrochemical impedance spectra (EIS) and equivalent circuits are shown in Fig. 9. The measurements were carried out with a fully charged state (4.35 V). An intercept in the high-frequency region of the Z_{rel} axis indicates the ohmic resistance (R_s), the combined resistance of the electrolyte, and the contacts of the cell [22]. The semicircle in the high–

Table 1 The average capacity retention

Times	The average capacity retention at 25 °C (%)	The average capacity retention at 45 °C (%)	The average capacity retention at 55 °C (%)	The average capacity retention at 65 °C (%)
1	94.4	93.5	93.6	91
2	93.8	94	94.4	89.8
3	94.2	94.3	93.8	91.2

Table 2 The amount of Mn^{2+} deposited on the Li anode after 100 cycles at 55±2 °C

Samples	The quality of Mn on the Li anode (μg/cm^2)
Pristine $LiMn_2O_4$	22.54
$LiNi_{1/3}Co_{1/3}Mn_{1/3}O_2$-coated $LiMn_2O_4$	10.17

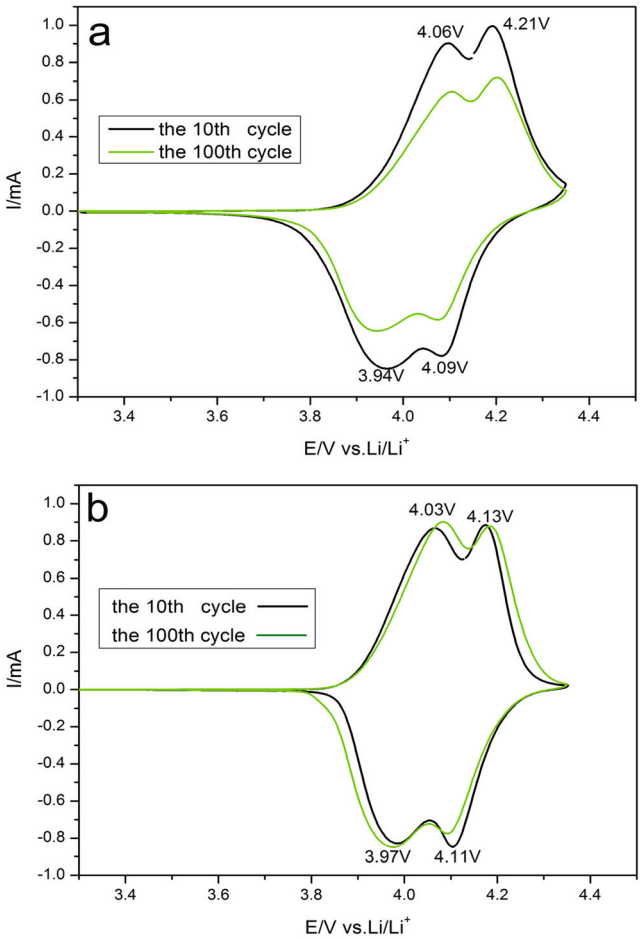

Fig. 8 Typical CV curves of the 10th and 100th cycles in a drying oven (55±2 °C) of **a** pristine and **b** $LiNi_{1/3}Co_{1/3}Mn_{1/3}O_2$-coated $LiMn_2O_4$

middle-frequency region corresponds to the charge transfer (R_{ct}) process on the electrode interface, revealing the lithium transfer rate parameters and the capacitance of the solid electrolyte interface (SEI) [23]. The inclined line in the lower

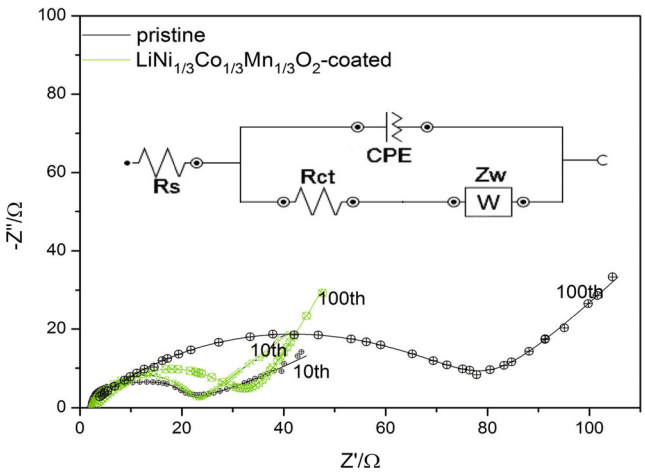

Fig. 9 EIS of pristine and $LiNi_{1/3}Co_{1/3}Mn_{1/3}O_2$-coated $LiMn_2O_4$ at the end of the 10th and 100th cycles

Table 3 The AC impedance fitting data for pristine $LiMn_2O_4$ and $LiNi_{1/3}Co_{1/3}Mn_{1/3}O_2$-coated $LiMn_2O_4$

Samples	R_s/Ω	R_{ct}/Ω
Pristine $LiMn_2O_4$ at the 10th fully charged state	2.01	26.80
$LiNi_{1/3}Co_{1/3}Mn_{1/3}O_2$-coated $LiMn_2O_4$ at the 10th fully charged state	1.86	22.4
Pristine $LiMn_2O_4$ at the 100th fully charged state	3.91	78.2
$LiNi_{1/3}Co_{1/3}Mn_{1/3}O_2$-coated $LiMn_2O_4$ at the 100th fully charged state	2.95	32.6

frequency region represents the Warburg impedance (Z_w), which corresponds to the diffusion of Li^+ in $LiMn_2O_4$ particles [24]. The plots are fitted and listed in Table 3. As shown in the table, after 10 cycles, the R_s of $LiNi_{1/3}Co_{1/3}Mn_{1/3}O_2$-coated $LiMn_2O_4$ is slightly larger than that of the pristine sample because the coating layer may slightly increase the electrolyte and contact resistance. The charge transfer resistance of both samples is approximately similar (26.8 and 22.4 Ω cm^2). After 100 cycles, the change in R_s is negligible. However, the R_{ct} value of the $LiNi_{1/3}Co_{1/3}Mn_{1/3}O_2$-coated electrode (32.6 Ω cm^2) is much smaller than that of the pristine electrode (78.2 Ω cm^2). It attributes to the restraint of structural instability caused by the subsequent Mn dissolution and vacancy formation. This result is also in accordance with the enhanced cycling performance of $LiNi_{1/3}Co_{1/3}Mn_{1/3}O_2$-coated electrodes.

Conclusions

In summary, the surface of the $LiMn_2O_4$ sample was modified by $LiNi_{1/3}Co_{1/3}Mn_{1/3}O_2$ using a sol–gel method. TEM and XPS results confirm the existence of the $LiNi_{1/3}Co_{1/3}Mn_{1/3}O_2$ layer. A uniform and dense layer about 5–6 nm was coated on the surface of pristine $LiMn_2O_4$. The $LiNi_{1/3}Co_{1/3}Mn_{1/3}O_2$-coated $LiMn_2O_4$ sample exhibits much better cycling stability at elevated temperature compared with the pristine sample. The CV tests indicated that the $LiNi_{1/3}Co_{1/3}Mn_{1/3}O_2$-coated $LiMn_2O_4$ electrode has better reversibility and stability. Meanwhile, the charge transfer resistance of the $LiNi_{1/3}Co_{1/3}Mn_{1/3}O_2$-coated $LiMn_2O_4$ was much less than that of the pristine sample after 100 cycles, which is ascribed to the better structural stability and restraint of Mn dissolution. These results demonstrated that this is an effective way to improve the high-temperature cyclic performance of spinel $LiMn_2O_4$.

Acknowledgments This work was supported by the National Science Foundation of China (No. 50672026). This work was also supported by the Shanghai Nanotechnology Promotion Center (No. 12ZR1448800)

References

1. Pitchai R, Thavasi V, Mhaisalkar SG, Ramakrishna S (2011) Nanostructured cathode materials: a key for better performance in Li-ion batteries. J Mater Chem 21(30):11040–11051
2. Zhao S, Bai Y, Ding LH, Wang B, Zhang WF (2013) Enhanced cycling stability and thermal stability of YPO_4-coated $LiMn_2O_4$ cathode materials for lithium ion batteries. J Solid State Ionics 247:22–29
3. Kim WK, Han DW, Ryu WH, Lim SJ, Kwon HS (2012) Al_2O_3 coating on $LiMn_2O_4$ by electrostatic attraction forces and its effects on the high temperature cyclic performance. J Electrochimica Acta 71:17–21
4. Arumugam D, Paruthimal Kalaignan G (2011) Electrochemical characterizations of surface modified $LiMn_2O_4$ cathode materials for high temperature lithium battery applications. J Thin Solid Films 520: 338–343
5. Li X (2012) Rui Yang etc, Enhanced electrochemical properties of nano-Li_3PO_4 coated on the $LiMn_2O_4$ cathode material for lithium ion battery at 55 °C. J Materials Letter 66:168–171
6. Kim D, Park S, Chae OB, Ryu JH, Kim YU, Yin RZ, Oh SM (2012) Re-deposition of manganese species on spinel $LiMn_2O_4$ electrode after Mn dissolution. J Electrochem Soc 159(3):A193–A197
7. Gummow RJ, Dekock A, Thackeray MM (1994) Improved capacity retention in rechargeable 4 V lithium/lithium manganese oxide (spinel) cells. J Solid State Ionics 69(1):59–67
8. Jang DH, Shin YJ, Oh SM (1996) Dissolution of spinel oxides and capacity losses in 4 V Li/$Li_xMn_2O_4$ coils. J Electrochem Soc 143(7): 2204–2211
9. Wu XL, Kim SB (2002) Improvement of electrochemical properties of LiNi(0.5)Mn(1.5)O(4) spinel. J Power Sources 109(1):53–57
10. Tarascon JM, Wang E, Shokoohi FK, Mckinnon WR, Colson S (1991) The spinel phase of $LiMn_2O_4$ as a cathode in secondary lithium cells. J Electrochem Soc 138(10):2859–2864
11. Hernan L, Morales J, Sanchez L, Santos J (1999) Use of Li-M-Mn-O [M=Co, Cr, Ti] spinels prepared by a sol-gel method as cathodes in high-voltage lithium batteries. J Solid State Ionics 118(3–4):179–185
12. Thackeray MM, Johnson CS, Kim JS, Lauzze KC, Vaughey JT, Dietz N, Abraham D, Hackney SA, Zeltner W, Anderson MA (2003) ZrO_2- and Li_2ZrO_3-stabilized spinel and layered electrodes for lithium batteries. J Electrochem Commun 5(9):752–758
13. Huang B, Li X, Wang Z, Guo H, Xiong X, Wang J (2014) A novel carbamide-assistant hydrothermal process for coating Al_2O_3. J Alloys Compd 583:313–319
14. Zheng ZH, Tang ZL, Zhang ZT, Shen WC, Lin YH (2002) Surface modification of $Li_{1.03}Mn_{1.97}O_4$ spinels for improved capacity retention. J Solid State Ionics 148(3–4):317–321
15. Gnanaraj JS, Pol VG, Gedanken A, Aurbach D (2003) Improving the high-temperature performance of $LiMn_2O_4$ spinel electrodes by coating the active mass with MgO via a sonochemical method. J Electrochem Commun 5(11):940–945
16. Wu F, Wang M, Su YF, Chen S, Xu B (2009) Effect of TiO2-coating on the electrochemical performances of $LiCo_{1/3}Ni_{1/3}Mn_{1/3}O_2$. J Power Sources 191(2):628–632
17. He XM, Li JJ, Cai Y, Wang YW, Ying JR, Jiang CY, Wan CR (2005) Preparation of co-doped spherical spinel $LiMn_2O_4$ cathode materials for Li-ion batteries. J Power Sources 150:216–222
18. Li X, Xu Y, Wang C (2009) Suppression of Jahn-Teller distortion of spinel $LiMn_2O_4$ cathode. J Alloys Compound 479:310
19. Kim WK, Dong H (2012) Al_2O_3 coating on $LiMn_2O_4$ by electrostatic attraction forces and its effects on the high temperature cyclic performance. J Eletrochemica Acta 71:17–21
20. L. F, S. W, Lu Han. Enhanced electrochemical properties of $LiMn_2O_4$ cathode material coated by 5wt.% of nano-La_2O_3, Journal of Materials Letters 78(2012) 116-119.
21. Liu D, He Z (2007) Increased cycling stability of $AlPO_4$-coated $LiMn_2O_4$ for lithium ion batteries. J Mater Letters 61: 4703–4706
22. Myung ST, Izumi K, Komaba S, Sun YK, Yashiro H, Kumagai N (2005) Role of alumina coating on Li-Ni-Co-Mn-O particles as positive electrode material for lithium-ion batteries. J Chem Mater 17(14):3695–3704
23. Jang SB, Kang SH, Amine K, Bae YC, Sun YK (2005) Synthesis and improved electrochemical performance of Al (OH)(3)-coated Li[$Ni_{1/3}Mn_{1/3}Co_{1/3}$]O_2 cathode materials at elevated temperature. J Electrochimica Acta 50(20):4168–4173
24. Levi MD, Gamolsky K, Aurbach D, Heider U, Oesten R (2000) On electrochemical impedance measurements of Lix$Co_{0.2}Ni_{0.8}O_2$ and LixNiO_2 intercalation electrodes. Electrochim Acta 45(11): 1781–1789

$LiNi_{1/3}Co_{1/3}Mn_{1/3}O_2$ is a new coating material on $LiMn_2O_4$. A uniform and dense layer about 5–6 nm was formed on the surface of $LiMn_2O_4$. The $LiNi_{1/3}Co_{1/3}Mn_{1/3}O_2$ coating layer significantly improves the high-temperature cycling stability of $LiMn_2O_4$.